44-Gb/s Silicon Microring Modulators Based on Zigzag PN Junctions

Xi Xiao, Xianyao Li, Hao Xu, Yingtao Hu, Kang Xiong, Zhiyong Li, Tao Chu, Jinzhong Yu, and Yude Yu

***Abstract*— We experimentally demonstrate silicon microring modulators with >40-Gb/s modulation speed based on the carrier-depletion mechanism in reverse-biased PN junctions. A novel zigzag PN junction providing a modulation efficiency of 3.85 × 10^{-5}/V and a resistance-capacitance bandwidth of 51 GHz is proposed and demonstrated. The moderate Q factor of ~8 000 and the operation wavelength detuning are optimized to relieve photon-lifetime-induced bandwidth limitation. Finally, with a voltage swing of 3 V, high-speed modulation of 20 and 44 Gb/s is experimentally demonstrated with the extinction ratio of 3.45 and 3.01 dB, showing great potential in the application of ultrahigh-capacity optical interconnects.**

***Index Terms*— High speed, microring resonator (MRR), optical modulation, silicon modulators.**

I. Introduction

HIGH-CAPACITY on-chip optical interconnects greatly desire a silicon-based modulator which offers high speed, compact footprint and low power consumption. Mach–Zehnder interferometers (MZI) and microresonators are two kinds of commonly used optical structures of silicon modulators. Although modulation speed up to 50 Gb/s has been demonstrated based on depletion-mode silicon MZI modulators [1], [2], their typical device sizes are normally on the scale of millimeter in order to produce enough phase shift for acceptable modulation depth [3]. Moreover, the power consumption needed to drive such a long phase shifter is normally difficult to satisfy the requirement of on-chip optical interconnects [4].

Microresonator-based modulators, such as micoring, microdisk and photonic crystal modulators, have been previously demonstrated with ultra-small size [5] and fJ/bit-scale power consumption [6]. However, their speeds are limited to less than 30 Gb/s due to the relatively long photon lifetime of high-Q resonators [7]. Although a kind of coupling-modulated microring resonator (MRR) modulator is proposed and demonstrated to overcome this photon lifetime limitation [8], its coupling region has a length of several hundred micron-meters which reduces the advantages of low-power and compactness over MZI modulators.

In this letter, we present a compact silicon MRR modulator with modulation speed up to 44 Gb/s. A novel zigzag PN junction with enhanced carrier-light interaction and 51 GHz electrical bandwidth is employed. The ring waveguide loss and the operation wavelength are both properly designed to obtain a moderate Q factor and a modulation bandwidth of ~25 GHz. Finally, clear opening eye-diagrams of 20 Gb/s and 44 Gb/s with reasonable extinction ratios are experimentally observed.

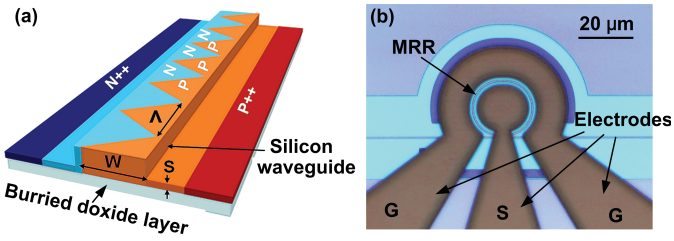

Fig. 1. (a) Schematic doping profile and waveguide structure. Waveguide width: W = 550. Slab thickness: S = 80 nm. Doping period of the zigzag PN junction: Λ = 600 nm. (b) Top-view microscope figure of the modulator after fabrication. The brown colored regions are aluminum ground-signal-ground electrodes.

II. Device Description and Fabrication

An efficient solution to overcome the cavity lifetime limitation is to improve the modulation efficiency, that is, to increase the resonance shift. This can be realized by employing a PN junction with enhanced electro-optical (E-O) interaction. We have proposed and demonstrated an interleaved PN junction to improve the light-carrier spatial overlap [9]. In this letter, we develop another kind of PN junction with a zigzag configuration in order to reduce the junction capacitance. As shown in Fig. 1(a), the junction is embedded into a 340 nm-high and 500 nm-wide rib waveguide which has an 80 nm-thick slab. The zigzag PN junction has a periodic doping period of $\Lambda = 600$ nm. The P- and N-type doping concentrations are both 2×10^{17} cm^{-3}. Highly doped N^{++} and P^{++} regions with the concentrations of $\sim 1 \times 10^{20}$ cm^{-3} are both located 500 nm away from each waveguide edge for ohmic contact to the 1 μm-thick aluminum electrodes with a 40 μm gap width at the contacting pads.

Manuscript received May 29, 2012; revised August 6, 2012; accepted August 31, 2012. Date of publication August 31, 2012; date of current version September 12, 2012. This work was supported in part by the National Basic Research Program of China under Grant 2011CB301701 and Grant 2012CB933502, and in part by the National Natural Science Foundation of China under Grant 60877036 and Grant 61107048.

The authors are with the State Key Laboratory on Integrated Optoelectronics, Institute of Semiconductors, Chinese Academy of Sciences, Beijing 100083, China (e-mail: xixiao@semi.ac.cn; xianyaoli@semi.ac.cn; xuhao@semi.ac.cn; ythu@semi.ac.cn; xiongkang@semi.ac.cn; lizhy@semi.ac.cn; tchu@semi.ac.cn; jzyu@semi.ac.cn; yudeyu@semi.ac.cn).

Color versions of one or more of the figures in this letter are available online at http://ieeexplore.ieee.org.

Digital Object Identifier 10.1109/LPT.2012.2213244

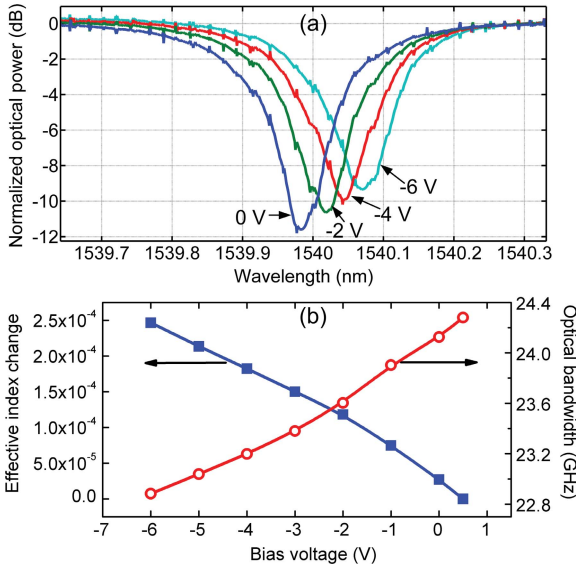

Fig. 2. (a) Measured resonance shifts. (b) Effective index change (blue) and optical bandwidth (red) under different bias voltages.

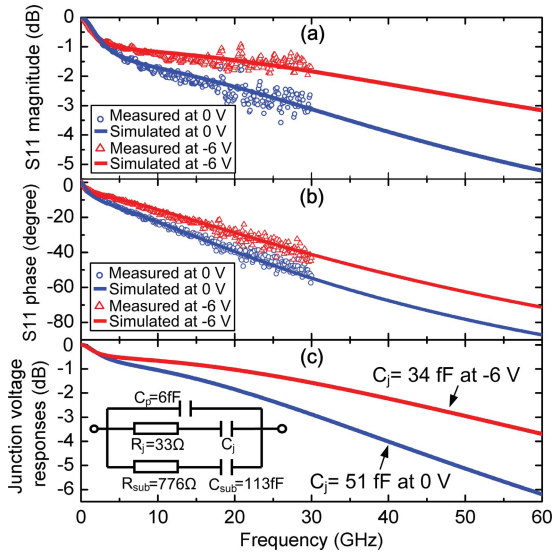

Fig. 3. Measured (dots) and fitted (lines) S11: (a) magnitude and (b) phase responses at 0 and −6 V, respectively. (c) Amplitude response of the voltage applied to the junction because of the equivalent circuit model shown in the inset.

The device fabrication, which was described in [10] in detail, was implemented in the standard 0.18 μm complementary-metal-oxide-semiconductor (CMOS) foundry at Semiconductor Manufacturing International Corporation (SMIC) in China. Figure 1(b) shows the top-view microscope image of a fully fabricated MRR modulator with single side coupled to a straight bus waveguide. The gap between the ring and bus waveguide is designed to be 200 nm-wide for the 0.18 μm-CMOS compatibility. The MRR is optimized to form a racetrack-shape with 10 μm bending radius and 2 μm-long straight waveguides. The racetrack configuration increases the coupling strength and introduces mode-conversion loss, which helps obtain a low-Q resonance with deep notch. The corners of the zigzag junction would be smoothed due to the lithography limitation and the dopant diffusion. However, the profile deformation occurs at the waveguide edges where the light intensity is low. So the fabrication actually introduces little variation on the modulation efficiency.

III. Device Characterizations

The modulator's DC performance was investigated by measuring the resonance shift with the bias voltages varying from 0.5 V to −6 V, as shown in Fig. 2(a). The average wavelength shifting efficiency is ∼16 pm/V which corresponds to an effective index change of 3.85×10^{-5}/V and a corresponding $V_\pi L_\pi$ of 1.7 V·cm, as shown in Fig. 2(b). Such a high modulation efficiency is realized by interleaving the junction interface which results in an enhanced light-carrier spatial overlap. The MRR modulator is under an over-coupling condition with the Q factor of 8015. As the electrical bandwidth of the reverse-biased PN junction is normally several tens of GHz, the photon-lifetime-limited bandwidth f_{opt} becomes the speed limitation. We approximately calculate the optical bandwidth from the measured Q factor according to the expression of $f_{opt} = \omega/2\pi Q$, where ω is the angular frequency. When increasing the reverse-bias voltage, the absorption loss reduces due to the carrier-depletion. The corresponding f_{opt} hence reduces from 24.3 GHz to 22.8 GHz, as shown in Fig. 2(b).

The electrical characteristics of the zigzag PN junction were both analyzed by the DC performance measurements and curve-fitting the dynamic frequency responses. Firstly, we measured the junction resistance and capacitance approximately to be 28 ± 5 Ω and 50 ± 10 fF by I–V and C–V characterizations, respectively. The other parameters can be extracted from the equivalent circuit model and the S11 curve fitting. The measured S11 magnitude and phase response are respectively shown in Fig. 3(a) and (b). The dots represent the measured results by using a calibrated signal integrity network analyzer from DC to 30 GHz. The lines represent the corresponding fitting curves simulated from the equivalent circuit model shown in the inset of Fig. 3(c). C_p, C_j and C_{sub} are the capacitances induced by the pads, PN junction and the Si substrate, respectively. R_j and R_{sub} are the resistance of the junction and the Si substrate, respectively. With voltage changes from 0 V to −6 V, the extracted C_j reduces from 51 fF to 34 fF due to the expansion of the depletion region. A method has been developed to investigate the intrinsic electrical bandwidth of the PN junction [10]. The amplitude responses of the voltage applied to the junction are shown in Fig. 3(c). The reduction of the junction capacitance is found to have great improvement on the device electrical 3-dB bandwidth. An electrical 3-dB bandwidth of ∼51 GHz is estimated at −6 V bias, which benefits from the low resistance-capacitance (RC) constant of the zigzag PN junction.

The modulation bandwidth also depends on the operation wavelength. The input light with wavelength closer to the resonance is easier to be trapped into the MRR and therefore has a longer photon lifetime. The E-O modulation bandwidths at different operating wavelengths are simulated by the time-domain transfer matrix method which contains all the optical and electrical parameters described above. The results are

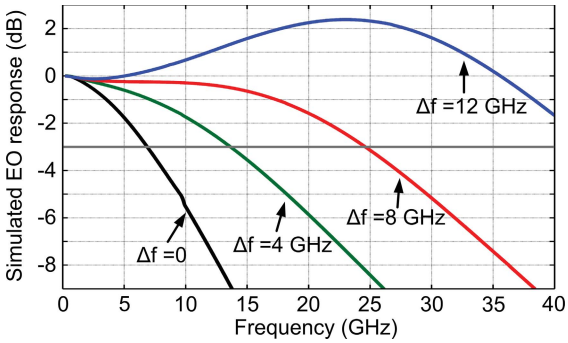

Fig. 4. Simulated E-O modulation responses at different operation wavelengths. Δf represents the frequency difference between the operating wavelength and the resonating wavelength.

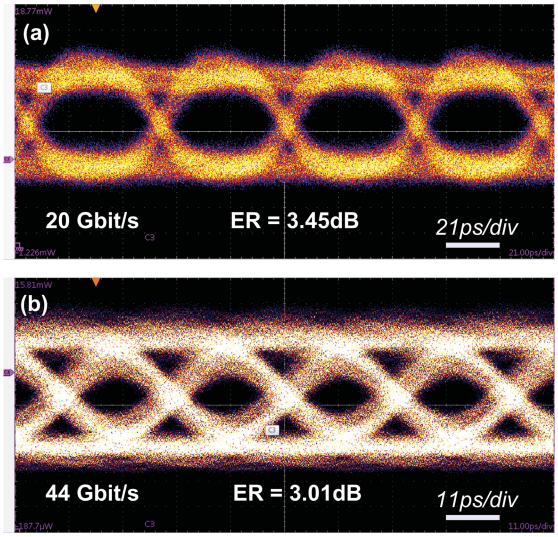

Fig. 5. (a) 20-Gb/s and (b) 44-Gb/s modulation eye-diagram driven by a PRBS $2^{31}-1$ signal with V_{pp} of 3 V and a DC bias of −3 V.

shown in Fig. 4, where Δf represents the frequency difference between the input light and the ring resonance. When the input light is on resonance (Δf = 0), the E-O bandwidth is only 6.9 GHz. When the wavelength is detuned by 4 GHz and 8 GHz, the E-O bandwidth would increase to 13.6 GHz and 24.6 GHz, respectively. When the Δf is set to 12 GHz, a peaking effect is found at high frequency which originates from the releasing of the light stored inside the MRR. This effect is associated with an overshoot at rising edges of the modulated output signal and has been demonstrated theoretically [11], [12] and experimentally [13]. Although simulations predict an E-O bandwidth much larger than the cavity linewidth by increasing the Δf, we need to choose a proper operating wavelength for a tradeoff between modulation speed and extinction ratio.

IV. High-Speed Modulation

To demonstrate the high-speed modulation, we carried out the eye-diagram measurements. The modulator was driven by a non-return-zero pseudorandom binary sequence (PRBS) 2^{31}–1 signal with a V_{pp} of 3 V and a DC bias of −3 V through a 40 GHz ground-signal-ground probe. Continuous-wave (CW) light with Δf ∼ 8 GHz was coupled into the modulator by a grating coupler. The modulated optical signal was then amplified by an erbium-doped fiber amplifier, filtered by a 0.8 nm band-pass filter and finally fed into the 65 GHz optical head on a Tektronix digital scope. Fig. 5(a) shows the measured modulation eye-diagram at 20 Gb/s with an extinction ratio (ER) of 3.45 dB. The modulation power consumption is estimated to be ∼300 fJ/bit because the driving voltage is doubled by the termination reflection. For the bit rate of 44 Gb/s in Fig. 5(b), the ER only decreases by ∼0.5 dB, indicating the capability of a higher modulation speed. Although the results are limited by our 44 Gb/s pattern generator, this is so far the fastest speed demonstrated by a silicon modulator based on MRR. The clear open eye-diagram also indicates the potential for error-free operation.

V. Conclusion

In conclusion, we demonstrated a compact silicon MRR modulator operating at a bit-rate of >40 Gb/s. By designing the 22 μm-long MRR's Q factor and employing a novel zigzag PN junction with modulation efficiency of 3.85×10^{-5}/V and estimated RC bandwidth of 51 GHz, we obtained a clear opening eye-diagram at 44 Gb/s with a 3.01 dB extinction ratio. A higher modulation speed can be expected based on the current device. Dramatic reduction on the driving voltage and the power consumption can be realized by optimizing the doping concentrations and employing the differentially signaled driving scheme [6], which remained as our future work.

References

[1] D. Thomson, *et al.*, "50 Gb/s silicon optical modulator," *IEEE Photon. Technol. Lett.*, vol. 24, no. 4, pp. 234–236, Feb. 15, 2012.
[2] P. Dong, L. Chen, and Y.-K. Chen, "High-speed low-voltage single-drive push-pull silicon Mach–Zehnder modulators," *Opt. Express*, vol. 20, no. 6, pp. 6163–6169, 2012.
[3] F. Y. Gardes, *et al.*, "High-speed modulation of a compact silicon ring resonator based on a reverse-biased PN diode," *Opt. Express*, vol. 17, no. 24, pp. 21986–21991, 2009.
[4] D. A. B. Miller, "Device requirements for optical interconnects to silicon chips," *Proc. IEEE*, vol. 97, no. 7, pp. 1166–1185, Jul. 2009.
[5] B. Schmidt, Q. Xu, J. Shakya, S. Manipatruni, and M. Lipson, "Compact electro-optic modulator on silicon-on-insulator substrates using cavities with ultrasmall modal volumes," *Opt. Express*, vol. 15, no. 6, pp. 3140–3148, 2007.
[6] W. A. Zortman, A. L. Lentine, D. C. Trotter, and M. R. Watts, "Low-voltage differentially-signaled modulators," *Opt. Express*, vol. 19, no. 27, pp. 26017–26026, 2011.
[7] J. C. Rosenberg, *et al.*, "Low-power 30 Gb/s silicon microring modulator," in *Proc. Lasers Electro Opt. Conf.*, May 2011, pp. 1–2, paper PDPB9.
[8] W. D. Sacher, *et al.*, "28 Gb/s silicon microring modulation beyond the linewidth limit by coupling modulation," in *Opt. Fiber Commun. Conf. OSA Tech. Dig.*, Mar. 2012, pp. 1–3, paper OM3J.2.
[9] Z.-Y. Li, *et al.*, "Silicon waveguide modulator based on carrier depletion in periodically interleaved PN junctions," *Opt. Express*, vol. 17, no. 18, pp. 15947–15958, 2009.
[10] X. Xiao, *et al.*, "25 Gb/s silicon microring modulator based on misalignment-tolerant interleaved PN junctions," *Opt. Express*, vol. 20, no. 3, pp. 2507–2515, 2012.
[11] W. D. Sacher and J. K. S. Poon, "Dynamics of microring resonator modulators," *Opt. Express*, vol. 16, no. 20, pp. 15741–15753, 2008.
[12] L. Zhang, Y. Li, J.-Y. Yang, M. Song, R. G. Beausoleil, and A. E. Willner, "Silicon-based microring resonator modulators for intensity modulation," *IEEE Sel. Topics Quantum Electron.*, vol. 16, no. 1, pp. 149–158, Jan. 2010.
[13] Q. Xu, S. Manipatruni, B. Schmidt, J. Shakya, and M. Lipson, "12.5 Gb/s carrier-injection-based silicon micro-ring silicon modulators," *Opt. Express*, vol. 15, no. 2, pp. 430–436, 2007.